MPOFI: Multichannel Partially Observed Functional Modeling for Defect Classification with Imbalanced Dataset via Deep Metric Learning

Yukun Xie, Juan Du*, Member, IEEE, Chen Zhang, Member, IEEE

Abstract—In modern manufacturing, most of the product lines are conforming. Few products are nonconforming but with different defect types. The identification of defect types can help further root cause diagnosis of production lines. With the sensing development, continuous signals of process variables can be collected in high resolution, which can be regarded as multichannel functional data. They have abundant information to characterize the process and help identify the defect types. Motivated by a real example from the pipe tightening process, we target at detect classification when each sample is a multichannel functional data. However, the available samples for each defect type are limited and imbalanced. Moreover, the functions are partially observed since the pre-tightening process before the pipe tightening process is unobserved. To classify the defect samples based on imbalanced, multichannel, and partially observed functional data is very important but challenging. Thus, we propose an innovative framework known as "Multichannel Partially Observed Functional Modeling for Defect Classification with an Imbalanced Dataset" (MPOFI). The framework leverages the power of deep metric learning in conjunction with a neural network specially crafted for processing functional data. This paper introduces a neural network explicitly tailored for handling multichannel and partially observed functional complemented by developing a corresponding loss function for training on imbalanced datasets. The results from a real-world case study demonstrate the superior accuracy of our framework when compared to existing benchmarks.

Note to Practitioners—This paper, motivated by the problem of identifying defect types in the pipe tightening process, focuses on developing accurate defect classification methods based on the multichannel functional data from sensor signals. Existing techniques to deal with multichannel functional data cannot deal with the partially observed functional data when the domain range of each function is unknown. Training the classification methods given an imbalanced industrial dataset is also challenging. To address the combined challenges, we develop a neural network to learn from the imbalanced, multichannel, and partially observed functional data. This is achieved by designing network structures

This work was supported in part by Guangdong Basic and Applied Basic Research Foundation (No. 2023A1515011656), Guangzhou Municipal Science and Technology Program under grant No. 202201011235, and the National Natural Science Foundation of China (No. 72001139 and No. 72371219). (Corresponding author: Juan Du).

Yukun Xie and Juan Du are with the Smart Manufacturing Thrust, Systems Hub, The Hong Kong University of Science and Technology (Guangzhou), Guangzhou 511400, China (e-mail: yukun.xie@connect.ust.hk; juandu@ust.hk).

Juan Du is also with the Department of Mechanical and Aerospace Engineering, The Hong Kong University of Science and Technology, Hong Kong SAR, China and Guangzhou HKUST Fok Ying Tung Research Institute, Guangzhou, China.

Chen Zhang is with the Department of Industrial Engineering, Tsinghua University, Beijing 100084, China (e-mail: zhangchen01@tsinghua.edu.cn).

that accept multichannel and varying-length functional data as input without specifying the domain ranges. A loss function is also proposed for the imbalance learning of the neural network. We provide practitioners with a guideline to tune the hyperparameters of our framework. The effectiveness of our framework has been validated by a real case, and the framework can be further applied to other manufacturing processes to deal with the multichannel functional data.

Index Terms—imbalanced classification, partially observed functional data, functional neural network, pipe tightening process

I. INTRODUCTION

HREADED pipes have extensive applications in various industries, particularly in petroleum wells and long-distance transportation. The paramount importance of high-quality threaded pipes [1] in ensuring safety during petroleum transportation is underscored by the fact that defective threaded pipes incur an annual cost of approximately half a billion USD [2]. Notably, a significant portion of the quality issues in threaded pipes arise from nonconforming connections. Thus, meticulous examination of the connection quality is a critical factor in determining the overall quality of threaded pipes.

The manufacturing process for threaded pipe connections depicted in Fig. 1 (a) encompasses a pre-tightening process followed by a pipe tightening process [3]. During the pre-tightening process, most threads are initially screwed, with the final connection achieved in the subsequent pipe tightening process. As depicted in Fig. 1 (b), sensors are positioned on pipe tightening machines to record process variables, including turns, torque, and tightening speed. These sensor signals provide a wealth of process-related information and reveal distinct phases, such as thread engagement, sealing, and shoulder contact, within the pipe tightening process. Consequently, the connection quality can be predicated on these sensor signals.

Currently, practitioners within the petroleum industry rely on torque-turn functions derived from sensor signals to manually label nonconforming pipe connections [1]. Assuming that the torque-turn functions are piecewise linear, based on physical analysis [4], practitioners manually identify the change points between different phases of the pipe tightening process, as illustrated in Fig. 2 (a). The torque values at these identified change points are then scrutinized against the specifications of the VAM connections [1]. However, manual labeling can only

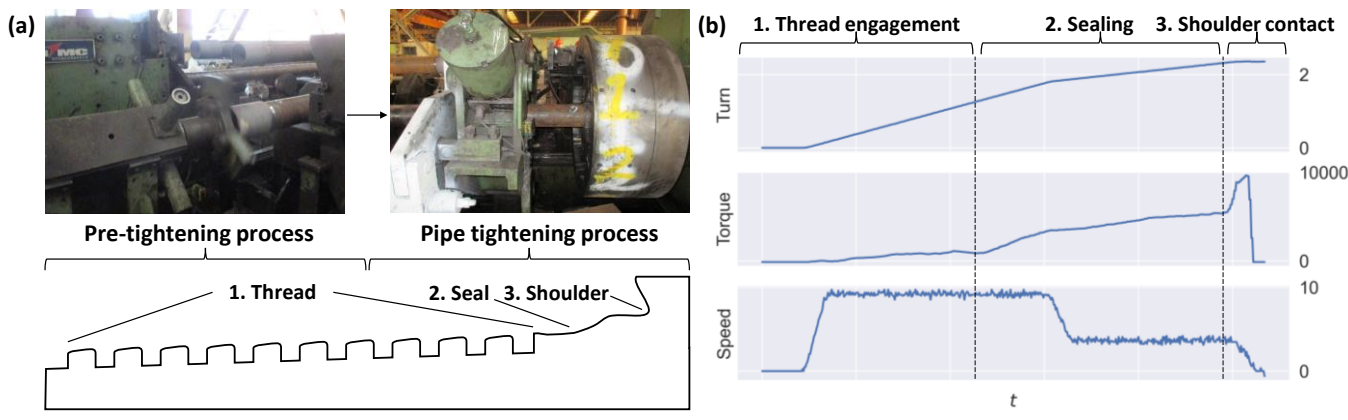


Fig. 1. (a) Manufacturing process and structure of threaded pipe connections [5]; (b) Sensor signals acquired in the pipe tightening process.

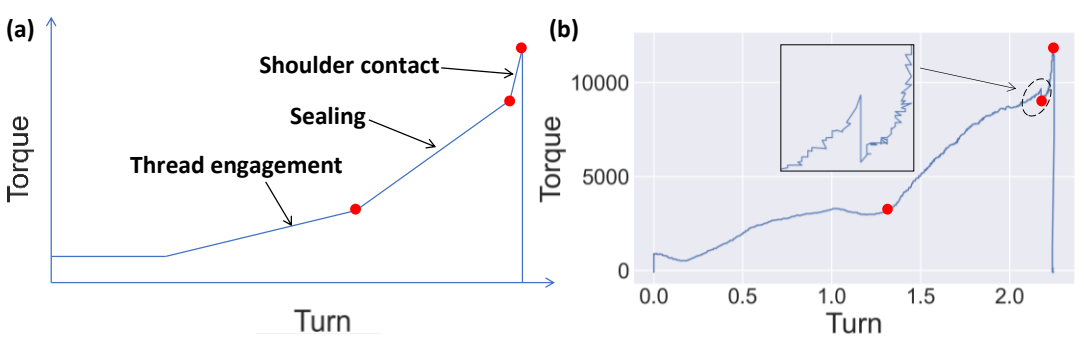


Fig. 2. (a) Physical pattern of torque-turn function; (b) Torque-turn function from real sensor signals.

determine whether a connection is nonconforming. It is necessary for expert intervention to further identify the defect type and implement appropriate remedial measures. In addition, it is essential to note that oscillations, as depicted in Fig. 2 (b), introduce challenges to current practices reliant on torque-turn functions. By directly using the data stream from sensors, which are functions over time t, the oscillations can be mitigated, presenting a more stable basis for quality assessment. Furthermore, this approach affords the opportunity to factor in the tightening speed, which has remained unaddressed in previous studies [1, 5-7]. Therefore, the establishment of a method based on the functional data of sensors is warranted to effectively identify nonconforming connections and their defect types, thereby enhancing manufacturing process efficiency and quality.

To construct the classification method, a dataset comprising multichannel functional data collected from sensors was assembled. However, the development of a classification method for this functional dataset presents the following three challenges:

1) Highly Imbalanced Dataset: The dataset is highly imbalanced, which is challenging for classification tasks. Owing to the stability of the manufacturing process, the dataset contains a limited number of nonconforming products. Consequently, the ratio between conforming and nonconforming products is highly skewed. Furthermore, the minority class labels suffer from data scarcity, potentially causing the classifier to overfit limited samples. Both label

imbalance and data scarcity pose significant challenges, such as overfitting, for the classification problem. The label distribution illustrated in Fig. 3 exemplifies the class imbalances in our case.

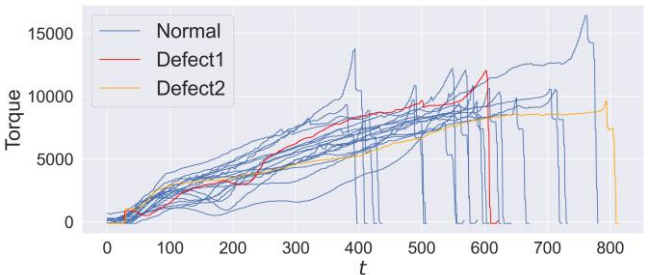


Fig. 3. 20 samples of torque-t function in our dataset.

- 2) Multichannel Functions: Each sample is a multichannel function due to multiple process variables collected by sensors. As illustrated in Fig. 1 (b), each channel exhibits a distinct range of values, with some ranging in tens and others in thousands.
- 3) Partial Observation of Processes: The incomplete observation of each process, particularly the unobserved pretightening process depicted in Fig. 1 (a), results in incomplete data reflecting the thread engagement phase. Traditional imputation or interpolation methods cannot effectively handle substantial and variable missing data segments within each function. Additionally, the inconsistency of the pre-tightening process results in varying-length observations for each pipe tightening process, as shown in Fig. 3. Thus, our method should

accurately classify each sample despite the partial observation of functional data.

The practical challenges described above are common in production lines, and the classification problem becomes even more challenging when the challenges are present simultaneously. The imbalanced classification problem needs to take into account the influence of learning from incomplete samples due to partial observability. Learning from multichannel functional data is also a novel topic in the context of imbalanced classification. Although there have been numerous studies on imbalanced classification in recent years, the applicability of these methods to functional data remains uncertain. In contrast, there has been a functional neural network [8] to learn from multichannel functions with varyinglength observations. Prior research in functional data analysis has also addressed challenges associated with partially observed functional data [9-12]. However, the methods assume that the domain range for each sample is known and require the pre-specification of domain ranges, which may not hold true for real production lines, such as the pipe tightening process in our case. Additionally, most existing classification methods in functional data analysis focus primarily on binary classification, with limited exploration of imbalanced multi-class classification problems. Consequently, our method endeavors to tackle the practical challenges presented by our dataset while leveraging existing research, including functional data analysis and classification of imbalanced datasets.

To overcome the challenges of classifying the imbalanced, multichannel, and partially observed functional data, we introduce a novel framework known as "multichannel partially observed functional modeling for defect classification with an imbalanced dataset" (MPOFI). Our modeling approach combines a functional neural network with deep metric learning. Specifically, a functional neural network is designed to directly learn fixed-length representations from multichannel functional data of varying lengths. To account for unobserved manufacturing processes, we employ a functional basis to pad the functional data before network encoding. In addition, we introduce a contrastive loss function tailored for deep metric learning on highly imbalanced functional datasets, thus facilitating efficient network training.

The contributions of our framework can be summarized as follows:

- 1) We propose a classification method for highly imbalanced functional data from manufacturing. By employing contrastive learning to address the imbalanced multi-class classification challenge, our MPOFI realizes the identification of nonconforming pipe connections and the classification of defect types.
- 2) With the application of functional neural networks, our framework can directly learn from the multichannel functional data. Our functional neural network surpasses traditional learning methods for functional data by enabling learnable and intricate transformations of functional data. Moreover, the convolution-based functional basis can directly encode

functional inputs without requiring pre-specification of domain ranges.

3) To handle the partially observed functional data, domain knowledge is incorporated into the padding mechanism of functional neural networks, thereby alleviating the influence of the unobserved parts of pipe tightening process.

The remainder of the paper is organized as follows. Section II conducts a literature review, encompassing methods for multichannel and partially observed functional data and learning strategies applicable to imbalanced datasets. Section III presents a detailed examination of the MPOFI framework, and Section IV offers an analysis of the evaluation results obtained from a real dataset of threaded pipe connections. Finally, Section V concludes the paper.

II. LITERATURE REVIEW

Our study is closely related to the methods used for imbalanced classification. In the realm of functional data analysis, methods to deal with multichannel functional data with partial observability are also relevant to our case. Thus, we review the current literature from two perspectives.

A. Imbalanced Classification

Considerable research has been dedicated to addressing the challenge of class imbalance when training neural networks using imbalanced datasets. This issue arises when there is a significant disparity between the number of samples in the majority and minority classes, leading to the decision boundary being skewed toward the majority labels. Traditional strategies for mitigating class imbalances can be broadly categorized into two groups: class rebalancing and data augmentation.

Class rebalancing methods aim to balance the influence of different labels on the decision boundary. A common approach involves employing various sampling strategies during training, such as random over sampling (creating additional samples from the minority class) and random under sampling (reducing the number of samples in the majority class). Another technique is cost-sensitive learning [13], with the representative method being focal loss [14], which assigns larger weights to the minority labels in the loss functions to emphasize their importance. Although the class rebalancing methods are effective for imbalanced classification, they may not be suitable when dealing with limited training samples, as is often the case in industrial data.

Data augmentation methods generate synthetic samples for minority labels to alleviate the imbalance problem. Examples of data generation methods include the synthetic minority oversampling technique (SMOTE) [15] and augmentation techniques tailored for time series or image data. In recent years, deep learning frameworks, such as autoencoders [16] and generative adversarial networks [17], have been applied to generate synthetic samples. However, these data augmentation methods may not be practical when training data are severely limited.

The class imbalance becomes even more challenging when dealing with a limited number of minority label samples, a

situation referred to as a "long-tailed dataset" [18]. Traditional strategies applied to such datasets can lead to overfitting of minority labels. In industrial data scenarios, where defect samples are scarce, data scarcity poses a problem. To address data scarcity, researchers have explored the application of transfer learning to detect defective samples [19]. In [19], the model was first pre-trained on the majority label and then transferred to the minority labels. However, pretraining models can be challenging in cases where samples have varying lengths and are only partially observed, as in our manufacturing dataset.

An alternative approach is deep metric learning, which decouples the imbalanced classification into two stages: representation learning and classifier training. During representation learning, an encoder maps input data into a discriminative feature space. In the subsequent classifier training stage, the classifier is trained based on the learned representations. A common method for representation learning is contrastive learning, which minimizes the distance between data representations from the same labels while maximizing the distance between data from different labels in the feature space. Existing studies have proposed losses based on contrastive learning to address imbalanced datasets [20-22]. However, these losses are primarily designed for image or speech data.

In our framework, we apply contrastive learning loss based on balanced contrastive learning [22] and N-pair loss [23]. Importantly, we modify the augmentation method used during the generation of the training samples to be suitable for functional data, aligning it with the characteristics of the manufacturing dataset.

B. Multichannel Functional Data with Partial Observability

For functions defined over a compact interval [a,b], it is common for observations from the function to be available only within a subset of [a,b]. The situation is similar to our threaded pipe connection case and clinical data [11,24]. Such datasets, known as partially observed functional data, are complete only within a specific interval $[a^*,b^*]$, where $a \le a^* < b^* \le b$. Approaches for handling partially observed and multichannel functional data can be categorized into three main groups: distance measure-based, reconstruction-based, and low-dimensional representation-based methods.

Distance measure-based methods quantify the dissimilarity between samples by defining distance measures. Typically, the distance measures are coupled with k-nearest neighbor (KNN) classifiers, which label a sample based on its proximity to labeled samples. One notable method in this category is dynamic time warping (DTW), which can be applied in our context. However, it is important to note that DTW was originally designed for sequence alignment, and its ability to represent differences between different labels in a multi-class classification may be affected. Another branch within this category is functional depth, which assesses the centrality of a sample within a set of labeled functions. Functional depth methods have been designed for partially observed functional data [24], and depth-based classifiers have proven effective in classifying functional data [25, 26]. Nevertheless, the Integrated Depth for Partially Observed Functional Data

(POIFD) [24] is unsuitable for our case because it requires a pre-specified domain range for each sample. Furthermore, POIFD only treats multichannel functional data as a weighted sum of univariate functions, with the weights also requiring prespecification.

Reconstruction-based methods aim to reconstruct the missing portions of a function and subsequently apply conventional classification techniques. Reconstruction is typically data-driven and can be based on fragments from other samples [10] or methods such as functional principal component analysis [11, 12]. However, a common limitation of these methods is that reconstruction does not always guarantee improved classification accuracy, especially in our scenario, where the sealing and shoulder contact phases exhibit most anomaly patterns, and only the thread engagement phase is incomplete. Since the domain range for the thread engagement phase is unknown for each function, reconstructing or deleting the observations for that phase is also impractical. Moreover, data-driven reconstruction cannot leverage the physical mechanisms of the manufacturing process.

In contrast to the above two categories, low-dimensional representation-based methods directly transform functional data into low-dimensional representations with fixed lengths. Beginning with pioneering work [9], various linear classifiers [27, 28] have been proposed. However, linear classifiers are not applicable because the assumptions of equal covariance for each label may not align with our dataset from the manufacturing process.

More recently, functional neural network approaches have shown promise for learning from functional data [8, 29]. With the power of neural networks, these approaches can directly encode multichannel functional data with varying-length observations and perform more intricate transformations of functional data, leading to improved discrimination results. A functional neural network is particularly suitable for our case because it can leverage label information and account for the label imbalance during training. However, current functional neural networks are typically based on multilayer perceptron (MLP), which lacks shift-invariance to functional input and necessitates pre-specification of the domain range. Therefore, modifications to the network structure are required to make it applicable in manufacturing cases, such as our pipe tightening process.

III. METHODOLOGY

In our specific industrial dataset, certain characteristics necessitate the direct learning of multichannel partially observed functional data without relying on model assumptions or requiring pre-specification of domain ranges. Additionally, the challenge posed by the imbalanced nature of the dataset should be addressed effectively. Therefore, there is a compelling need for a learning method tailored to the nuances of partially observed and imbalanced functional data derived from manufacturing processes.

Our MPOFI framework considers the underlying physical mechanisms of the manufacturing process and presents a neural

network designed to encode multichannel and partially observed functional data directly. The core of the framework is a functional neural network-based encoder capable of transforming sensor-derived functional data into low-dimensional features. Notably, the encoder can be trained to ensure that the resulting features are discriminative across different labels. To address the challenges associated with the imbalanced nature of the dataset, we introduced a contrastive learning-based deep metric learning framework. The

framework facilitates the training of the encoder using a highly imbalanced dataset, ultimately leading to a feature space in which defect classification can be performed effectively.

Section III-A introduces the general framework of MPOFI. The functional neural network used to encode multichannel and partially observed functional data is elaborated in Section III-B, and the contrastive loss designed for the imbalanced functional dataset is presented in Section III-C. In Section III-D, we provide guidelines for tuning the hyperparameters of MPOFI.

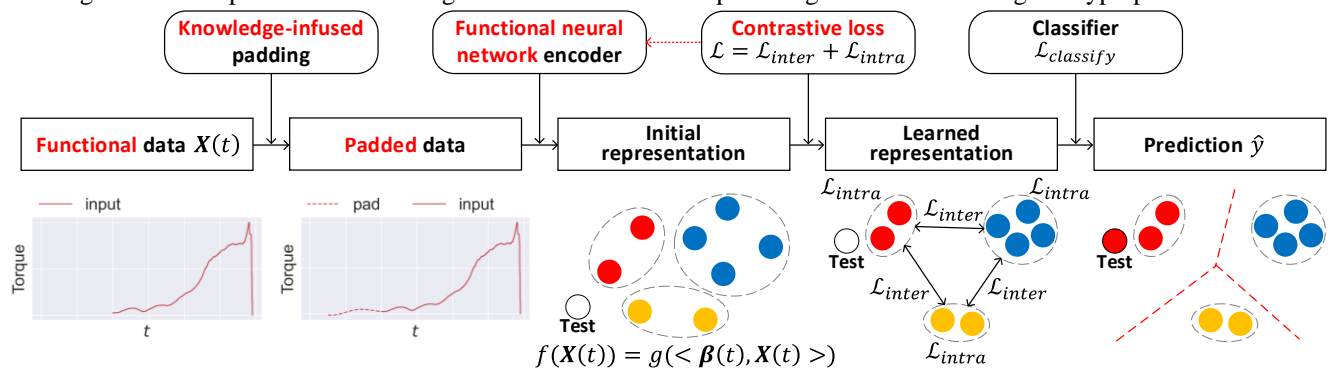


Fig. 4. Flowchart of the MPOFI framework.

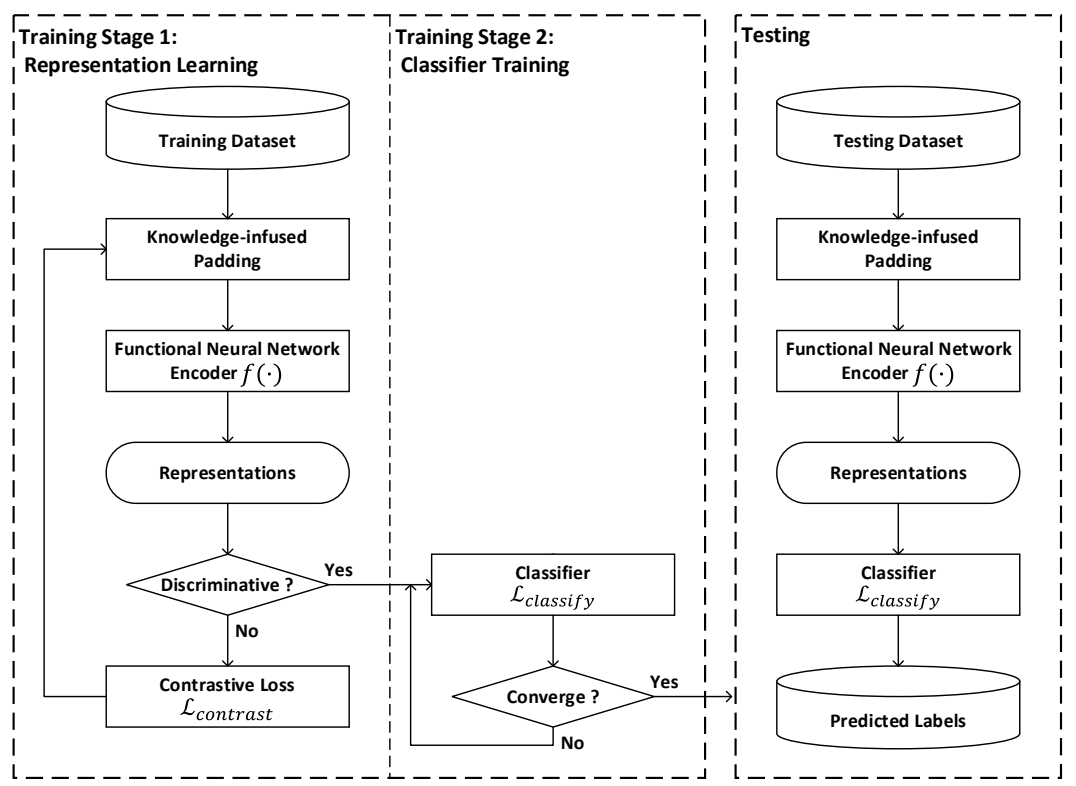


Fig. 5. Illustration of the MPOFI workflow.

A. General Framework

This section introduces the proposed MPOFI framework for the classification of imbalanced and partially observed functional data. We use X(t) to denote one sample of functional data, and $X(t) \in \mathbb{R}^{C \times T}$, t = 1, ..., T has C channels and T observations. The general framework follows the

paradigm of deep metric learning: each functional datum X(t) is first encoded into a low-dimensional representation and then classified based on discriminative representation. As shown in Fig. 4, X(t) first undergoes knowledge-infused padding, which reconstructs the padded area required for the neural network. The proposed functional neural network encoder $f(\cdot)$ then derives a fixed-dimensional representation f(X(t)). The initial

representations of the samples from the different labels are mixed in the feature space. Therefore, a contrastive loss $\mathcal{L}_{contrast}$ is proposed, and the encoder $f(\cdot)$ is trained through backpropagation. After the representation learning step, the learned representations under the same label are pulled together and the learned representations between different labels are pushed away. Finally, classifier $\mathcal{L}_{classify}$ is used to label f(X(t)) in the feature space.

The three modules, namely knowledge-infused padding, functional neural network encoder $f(\cdot)$, and contrastive loss $\mathcal{L}_{contrast}$, constitute the representation learning stage of the deep metric learning framework. In the classifier training stage, a classifier, such as a support vector machine (SVM), is trained on representations obtained after the representation learning stage. The functional neural network encoder $f(\cdot)$ and classifier after training are then used to predict the unlabeled samples. The overall workflow is illustrated in Fig. 5.

It should be noted that the proposed functional neural network and contrastive loss can work collaboratively and enhance the performance of each other. The padding mechanism of a functional neural network considers the physical mechanism of the manufacturing process, which guarantees that the padded values do not introduce bias to the functional input or subsequent contrastive loss. In return, contrastive loss enables the parameter updating of the functional neural network and improves the ability of the network to transform functional data after each iteration.

B. Functional Neural Network

As mentioned in Section II-B, existing MLP-based functional neural networks [8, 29] are not applicable in our case because the domain range for each function is unknown owing to partial observability. The neural network encoder should be shift-invariant and able to accept functions with different ranges and lengths as inputs. Therefore, we developed a functional neural network based on dilated convolution [30] and knowledge-infused padding.

The benefits of dilated convolution include shift-invariant features guaranteed by the convolution mechanism and the ability to accept varying-length inputs through dilated convolution. Assuming a dilation convolution layer with kernel size k_w and dilation size d and that the dilation is doubled for each layer, a convolution filter is applied over the input and skip input values with step 2^d . The receptive field grows exponentially with d, and the output length of the dilated convolution is still the input length T. Thus, the dilated convolution can use functional data X(t) with varying-length observations as the input.

Although dilated convolution has shown promise for handling functional data of varying lengths, the padding mechanism remains a challenge. Traditional padding methods can introduce bias into the distribution of functions, which can negatively affect the performance of the neural networks. Another challenge is designing a functional neural network with dilated convolution as the basic module. We illustrate the

proposed solution for the two challenges in Section III-B (a) and (b).

(a) Knowledge-infused Padding

In our case, the potential bias introduced by padding is a significant concern because the padding length increases exponentially with the dilation size in the dilated convolution. For example, the padding length is $(k_w - 1)2^d$ for dilation size d when dilation is doubled for each layer. Therefore, the padded values will significantly influence the original distribution of the functional data. To address the problem, we propose a novel approach called knowledge-infused padding. Similar to the reconstruction-based methods introduced in Section II-B, our knowledge-infused padding attempts to reconstruct functions with a functional basis to generate the padded data. The selection of bases is a critical factor that directly affects the padding quality. Therefore, in this study, the selection of the functional basis is based on the physical mechanisms of the manufacturing process.

Compared with the reconstruction-based method, the reconstruction area in our framework is only the padded part in the convolution, rather than the entire missing part. The reason is that we assume the most discriminative patterns exist in the common domain, which is complete for every sample. After specifying the basis functions $\{\phi_{(q)}(t)\}, g = 1, ..., G$, the knowledge-infused padding module is given in Algorithm 1 for any convolution layer with kernel size k_w and dilation size d.

Algorithm 1: Knowledge-infused Padding

Input: Functional data X(t), t = 1, ..., T; Convolution layer with kernel size k_w and dilation size d; Average pooling layer with kernel size k_w ; Basis functions $\{\phi_{(a)}(t)\}, g =$

Output: Padded data X'(t)

Obtain smoothed function X(t)

$$\overline{X}(t) = \frac{1}{k_w} \sum_{s=t}^{t+k_w} X(t), t = 1, \dots, T - k_w$$

Fit the basis expansion

$$\overline{X}(t) = \sum_{g=1}^{G} c_g \boldsymbol{\phi}_{(g)}(t)$$

Interpolate $\overline{X}(t)$ to length $T' = T + 2(k_w - 1)2^d$

Obtain the padded data X'(t)

$$X'(t) = \overline{X}(t), t = 1, ..., (k_w - 1)2^d$$

$$X'(t) = X(t), t = 1 + (k_w - 1)2^d, ..., T' - (k_w - 1)2^d$$

$$X'(t) = \overline{X}(t), t = T' - (k_w - 1)2^d, ..., T'$$

$$X'(t) = X(t), t = T' - (k_w - 1)2^d, ..., T'$$

(b) Network Structure

To encode the functional data $X(t) \in \mathbb{R}^{C \times T}$ for downstream classification tasks, the encoder should consider the functional data structures while ensuring that the entire encoder is trained to extract the discriminative features. Our proposed functional neural network $f(\cdot)$ achieves this by utilizing dilated convolution as the foundational structure. The details of the network structure are shown in Fig. 6.

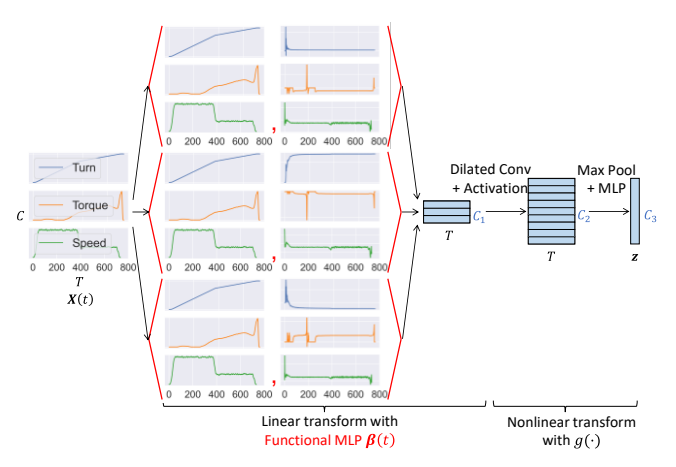


Fig. 6. Structure of the functional neural network $f(\cdot)$.

Given the final representation size C_3 , the network shown in Fig. 6 directly encodes the function $X(t) \in \mathbb{R}^{C \times T}$ to obtain the representation $\mathbf{z} \in \mathbb{R}^{C_3 \times 1}$ after knowledge-infused padding. Specifically, the network is composed of two parts: a linear transform with the basis layer $\beta(t)$ and a nonlinear transform with a traditional neural network $g(\cdot)$.

The basis layer $\beta(t)$ is implemented by stacking D dilation convolution layers without activation and performs similarly to the Functional MLP structure in [8]. The output for X(t)encoded by $f(\cdot)$ can be formulated as f(X(t)) = g(< $\beta_{(c)}(t), X(t) >$), $c = 1, ..., C_1$. The essence of the functional structure lies in the dilated convolution modules; the procedures are shown in Algorithm 2.

Algorithm 2: Functional MLP $\beta(t)$ based on dilated convolution

Input: Functional data
$$X(t)$$
; D layers of dilated convolution $\left\{b_{(c)}^{(l)}(t), h_{(c)}^{(l)}(t)\right\}$, $c=1,...,C_1, l=0,...,D-1$;

Output: $< \beta_{(c)}(t), X(t) >$

For $c=1:C_1$ do

 $u_{(c)}^{(0)}(t) = b_{(c)}^{(0)}(t) + h_{(c)}^{(0)}(t)X(t)$

End for

For $l=1:D-1$ do

For $c=1:C_1$ do

 $u_{(c)}^{(l)}(t) = b_{(c)}^{(l)}(t) + h_{(c)}^{(l)}(t)u_{(c)}^{(l-1)}(t)$

End for

End for

End for

 $< \beta_{(c)}(t), X(t) >= u_{(c)}^{(D-1)}(t), c=1,...,C_1$

As shown in Algorithm 2, we do not add activation functions for the D layers of the dilated convolution $\{\boldsymbol{b}_{(c)}^{(l)}(t), \boldsymbol{h}_{(c)}^{(l)}(t)\}$, which means that the entire structure does not contain nonlinearity and can be transformed into an MLP structure. By transforming the convolution weights $h_{(c)}^{(l)}(t)$ into a Toeplitz matrix and bias $b_{(c)}^{(l)}(t)$ as a vector, we can derive < $\boldsymbol{\beta}_{(c)}(t), \boldsymbol{X}(t) >= \boldsymbol{u}_{(c)}^{(D-1)}(t) = \boldsymbol{b}_{(c)}(t) + \boldsymbol{H}_{(c)}(t)\boldsymbol{X}(t). \ \boldsymbol{b}_{(c)}(t)$

$$\mathbf{b}_{(c)}(t), \mathbf{h}(t) \ge \mathbf{u}_{(c)}(t) + \mathbf{h}_{(c)}(t), \mathbf{h}(t) \cdot \mathbf{b}_{(c)}(t)$$
and $\mathbf{H}_{(c)}(t)$ are derived as follows:
$$\mathbf{b}_{(c)}(t) = \mathbf{b}_{(c)}^{(D-1)}(t) + \mathbf{h}_{(c)}^{(D-1)}(t) \times \mathbf{b}_{(c)}^{(D-2)}(t) + \cdots$$

$$+ \prod_{l=1}^{D-1} \mathbf{h}_{(c)}^{(l)}(t) \times \mathbf{b}_{(c)}^{(0)}(t), \qquad (1)$$

$$\mathbf{H}_{(c)}(t) = \mathbf{h}_{(c)}^{(D-1)}(t) \times \cdots \times \mathbf{h}_{(c)}^{(0)}(t), \qquad (2)$$

Matrix $H_{(c)}(t)$ is the Toeplitz matrix for all D convolution layers and can be viewed as a matrix basis. Therefore, the output of the Functional MLP layer $\beta(t)$ is functional data. The basis layer $\beta(t)$ based on convolution also makes the network shift-invariant to the input functions. Compared with the MLPbased functional neural network [8, 29], $\beta(t)$ can accept the functional input without specifying the domain range because the convolution can adapt to an input of any length.

Moreover, we can interpret the C_1 channels of group convolution as C_1 functional bases. Similar to traditional functional modeling with a set of bases [31], C_1 functional bases $\beta(t)$ can be interpreted well through visualization and identification of the most important bases.

After transforming $X(t) \in \mathbb{R}^{C \times T}$ into $\langle \boldsymbol{\beta}_{(c)}(t), X(t) \rangle \in$ $\mathbb{R}^{C_1 \times T}$ with basis layers, the neural network $g(\cdot)$ further transforms $\langle \boldsymbol{\beta}_{(c)}(t), \boldsymbol{X}(t) \rangle$ into $\mathbf{z} \in \mathbb{R}^{C_3 \times 1}$ through a convolution layer with C_2 channels and a $C_2 \times C_3$ MLP structure. The procedure for nonlinear transformation $g(\cdot)$ is shown in Algorithm 3. The representation z is then used to calculate the loss functions in Section III-C.

Algorithm 3: Nonlinear transformation $g(\cdot)$

Input: Out $\langle \boldsymbol{\beta}_{(c)}(t), \boldsymbol{X}(t) \rangle$ after linear transformation; convolution $\{\boldsymbol{b}_{(c)}^{(D)}(t), \boldsymbol{h}_{(c)}^{(D)}(t)\}, c = 1, ..., C_2 ;$ AdaptiveMaxPooling layer; MLP layer with weights \mathbf{R} , bias **E**, and activation σ ;

Output: z For c = 1: C_2 do $v_1 \in \mathbb{R}^{1 \times T} = \boldsymbol{b}_{(c)}^{(D)}(t) + \boldsymbol{h}_{(c)}^{(D)}(t) < \boldsymbol{\beta}_{(c)}(t), \boldsymbol{X}(t) > 0$ $\begin{aligned} & \boldsymbol{v}_2 \in \mathbb{R}^{C_2 \times T} = \text{LeakyReLU}(\boldsymbol{v}_1) \\ & \boldsymbol{v}_3 \in \mathbb{R}^{C_2 \times 1} = \text{AdaptiveMaxPool}\left(\boldsymbol{v}_2\right) \end{aligned}$ $\mathbf{z} \in \mathbb{R}^{C_3 \times 1} = \sigma(\mathbf{R} \mathbf{v}_3 + \mathbf{E})$

The details and proofs for constructing the Toeplitz matrix form of $h_{(c)}^{(l)}(t)$ and $H_{(c)}(t)$ are provided in the Appendix. Guidelines for setting hyperparameters D, C_1, C_2, C_3 are also provided in Section III-D.

C. Contrastive Loss

To train the functional neural network $f(\cdot)$ in Section III-B, a loss function should be proposed for tackling label imbalance and data scarcity issues when learning from the highly imbalanced functional dataset. We employ deep metric learning to train $f(\cdot)$, and the contrastive loss $\mathcal{L}_{contrast}$ is used.

Suppose that a dataset with J labels is denoted by $\{X_{ij}(t)\}, i = 1, ..., N_i, j = 1, ..., J$, where N_i is the sample size for label j. We first generate a mini-batch $\{X_{ij}(t)\}, i =$ $1, \dots, M_i, j = 1, \dots, J$ in each epoch through stratified sampling, where $M_1/N_1 = \cdots = M_j/N_j$. $\mathcal{L}_{contrast}$ is then calculated after for $\mathcal{L}_{contrast}$ is given in Equation (3-5):

all samples in the mini-batch are encoded by $f(\cdot)$. The formula

$$\mathcal{L}_{contrast}(\{X_{ij}(t)\}) = \mathcal{L}_{inter}\left(\{X_{j}^{*}(t), X_{j}^{+}(t), \{X_{k\neq j, l}^{-}(t)\}_{l=1}^{M_{k}-1}\}_{j=1}^{J}\right) + \mathcal{L}_{intra}\left(\{X_{j}^{*}(t), X_{j}^{+}(t)\}_{j=1}^{J}\right), \tag{3}$$

$$\mathcal{L}_{inter}\left(\left\{X_{j}^{*}(t), X_{j}^{+}(t), \left\{X_{k \neq j, l}^{-}(t)\right\}_{l=1}^{M_{k}-1}\right\}_{j=1}^{J}\right) = \frac{1}{J} \sum_{j=1}^{J} log\left(1 + \sum_{k \neq j} \frac{1}{M_{k} - 1} \sum_{l=1}^{M_{k}-1} \frac{exp\left(f\left(X_{j}^{*}(t)\right)f\left(X_{k, l}^{-}(t)\right)\right)}{exp\left(f\left(X_{j}^{*}(t)\right)f\left(X_{j}^{+}(t)\right)\right)}\right), \tag{4}$$

$$\mathcal{L}_{intra}\left(\left\{\boldsymbol{X}_{j}^{*}(t), \boldsymbol{X}_{j}^{+}(t)\right\}_{j=1}^{J}\right) = \frac{1}{J} \sum_{j=1}^{J} log \left(1 + \frac{1}{|Q|} \sum_{q \in Q} \frac{1}{exp\left(f\left(q\left(\boldsymbol{X}_{j}^{*}(t)\right)\right) f\left(q\left(\boldsymbol{X}_{j}^{+}(t)\right)\right)\right)}\right). \tag{5}$$

As shown in Equation (3), $\mathcal{L}_{contrast}$ is composed of an inter-class loss \mathcal{L}_{inter} and an intra-class \mathcal{L}_{intra} . Considering the imbalanced distribution of labels, \mathcal{L}_{inter} in Equation (4) is a modified N-pair loss [23] that distinguishes the representations between imbalanced labels. For each label j in the mini-batch $\{X_{i,j}(t)\}, i = 1, ..., M_i, j = 1, ..., J$, one anchor sample $X_i^*(t)$ and one positive sample $X_i^+(t)$ are randomly selected without replacement. All other samples from label $k \neq j$ are selected as negative samples $X_{k,l}^{-}(t)$ if they are not selected as anchor sample $X_k^*(t)$. Therefore, $\sum_{k \neq j} M_k$ contrasts are made for each label. In each contrast, the representations of $X_k^*(t)$ and $X_{k,l}^-(t)$ are pushed away, and the representations of $\boldsymbol{X}_{k}^{*}(t)$ and $\boldsymbol{X}_{k}^{+}(t)$ are pulled together. The reweighting term $\frac{1}{M_k-1}$ is added to Equation (4) to balance the contribution to \mathcal{L}_{inter} from the imbalanced labels.

Regarding the data scarcity issue, we propose an intra-class loss \mathcal{L}_{intra} in Equation (5) to avoid overfitting. To obtain more samples under one label, we augment the anchor sample $X_i^*(t)$ and positive sample $X_i^+(t)$ by applying a smoothing kernel q. Kernel $q \in Q$ is implemented through the average pooling layers with kernel size k_a , and we can set kernel set Q in advance. In contrast to \mathcal{L}_{inter} , the contrast pairs in \mathcal{L}_{intra} are limited to samples within the same label and are applied using the same smoothing kernel.

$$\begin{split} q\left(\pmb{X}_{j}^{*}(t)\right) &= \frac{1}{k_{q}} \sum_{s=t}^{t+k_{q}} \pmb{X}_{j}^{*}(t), t = 1, \dots, T - k_{q}, \quad (6) \\ q\left(\pmb{X}_{j}^{+}(t)\right) &= \frac{1}{k_{q}} \sum_{s=t}^{t+k_{q}} \pmb{X}_{j}^{+}(t), t = 1, \dots, T - k_{q}. \quad (7) \end{split}$$

D. Hyperparameter Tuning

In this section, we present the guidelines for tuning the hyperparameters in our MPOFI framework. hyperparameters include D, C_1 , C_2 , C_3 in the functional neural network $f(\cdot)$ and the kernel set Q in the contrastive loss $\mathcal{L}_{contrast}$.

The number of convolution layers D and the number of bases C_1 determine the performance of basis layer $\beta(t)$. The ability to fit complex functions increases with increasing D, whereas the padded length 2^D grows exponentially with D. Therefore, D is set to satisfy the requirement that the padded length should not exceed the raw data length $2^{D} < \min \{T_{ij}\}/$ $2, i = 1, ..., M_i, j = 1, ..., J$. The number of bases C_1 can first

be set as an initial value I * C * S, where S is the number of estimated piecewise linear segments for one function. During training, additional bases among the C_1 bases can be pruned by adding a channel-wise attention module to the neural network $f(\cdot)$. Channels C_2 and C_3 are the parameters for the traditional neural network $g(\cdot)$, and the network structure is the same as in previous practice [32]. Therefore, C_2 and C_3 can be set using the same settings as [32].

The setting of smoothing kernels $q \in Q$ can follow the procedure of smoothing functional data with a roughness penalty introduced in [31].

IV. EVALUATION

In this section, we apply the proposed MPOFI framework to a real dataset obtained from the manufacturing of threaded pipe connections to demonstrate its effectiveness. A total of 658 samples are manually labeled by the manufacturer, including normal connections and two types of nonconforming threaded pipe connections. The dataset has a substantial class imbalance, with 599 samples for normal connections, 28 samples for one defect type, and 31 samples for another defect type. As introduced in Section I, each sample is characterized by multichannel functional data, with partial observations occurring during the thread engagement phase of the manufacturing process.

To configure our MPOFI framework, we first select the basis functions for the knowledge-infused padding introduced in Section III-B (a). Taking the torque function in the manufacturing process as an example, we select the Fourier basis because the missing thread engagement process exhibits a periodic pattern. The results obtained using the Fourier basis and other traditional padding methods are shown in Fig. 7. Compared with traditional padding methods, our knowledgeinfused padding does not affect the distribution of the original functions. Similarly, we select the monomial basis for the turns and tightening speed functions in the manufacturing process since both the turns and tightening speed during the thread engagement process can be approximated with polynomials.

The other hyperparameters are set as follows: we set the number of bases $C_1 = 40$, following the guidelines outlined in Section III-D. The choice is based on the estimation of 3 * 3 *4 = 36 segments. The number of channels for other parts of the neural network, denoted as $C_2 = 160$, $C_3 = 320$, is consistent with the values used in [32]. The number of convolution layers D is set to 4, and average pooling kernels of size $\{1,3,5\}$ are used in Q.

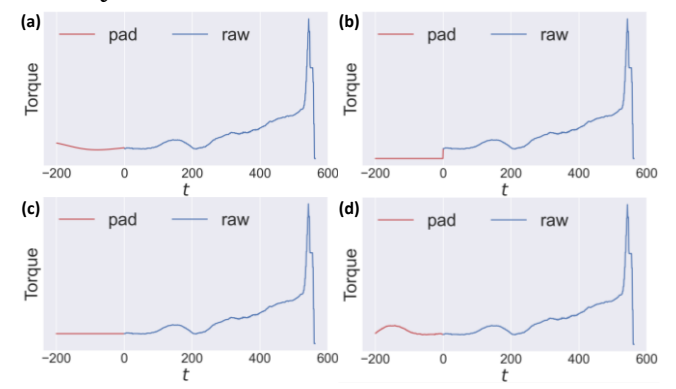


Fig. 7. Padding results obtained using different padding methods. (a) Knowledge-infused padding; (b) Zero padding; (c) Replication padding; (d) Reflective padding.

To demonstrate the efficacy of our MPOFI framework when dealing with partially observed and imbalanced functional data, we visualize the representations of functional data, as shown in Fig. 8. The fixed-dimensional representations are initially obtained from the multichannel and partially observed functions using functional neural networks, and are then visualized using the t-SNE technique [33]. We present the results from both the untrained network and the network after training to demonstrate the impact of representation learning. Fig. 8 (a) illustrates that representations from different functional data samples are mixed in the feature space when using an untrained network. However, after representation learning through training with the contrastive loss in Section III-C, the representations, as depicted in Fig. 8 (b), become distinctly separated in the feature space. The separation facilitates subsequent classification, demonstrating that MPOFI enables the accurate classification of partially observed and imbalanced functional data.

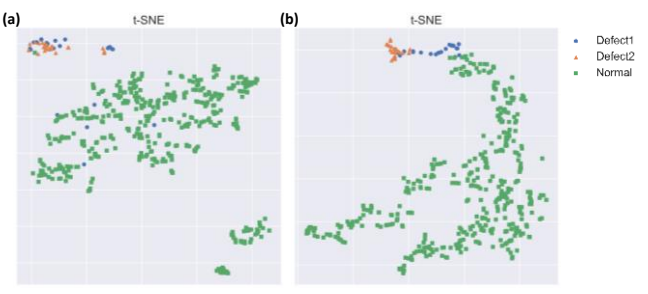


Fig. 8. Visualization of the representations with t-SNE. (a) Representations from the untrained functional neural network. (b) Representations from the functional neural network after training.

For comparison, we select three benchmark methods, each representing one of the categories introduced in Section II-A. The baseline method for classifying the functional data is DTW combined with a KNN classifier. Additionally, we utilize

POIFD [24], a benchmark method for evaluating functional depth, which considers partial observability. To apply POIFD to our dataset, we use the R package proposed in [24] to calculate depth measures and implement a depth-based classifier following [26]. Sparse functional linear discriminant analysis (SFLDA) [28] is chosen as a representative low-dimensional representation-based method, and its implementation is based on the open code available in [28]. To ensure fair comparisons, we adopt the same SVM classifier as the backbone for classifier training in both MPOFI and the depth-based classifier using POIFD.

To evaluate the performance, we employ balanced accuracy and macro-F1 as evaluation metrics, which are commonly used for imbalanced classification. The average results of 5-fold cross-validation using MPOFI and competing methods are presented in Table I.

TABLE I

COMPARISON OF PERFORMANCE ON THE THREADED PIPE

CONNECTION DATASET

Framework	Balanced Accuracy	Macro-F1
DTW+KNN	0.750	0.744
POIFD	0.732	0.745
SFLDA	0.816	0.814
MPOFI	0.939	0.939

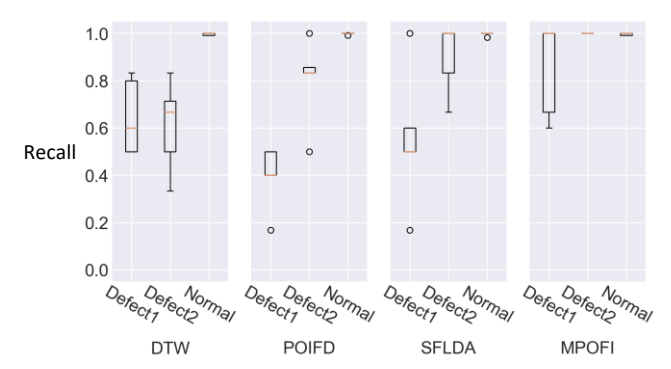


Fig. 9. Comparison of recall rates for each label.

As shown in Table I, our proposed MPOFI framework outperforms the competing methods in terms of both balanced accuracy and macro-F1 metrics. To provide a more detailed analysis of the classification accuracy, we present a boxplot of the results obtained from 5-fold cross-validation in Fig. 9. The recall rates for each label are displayed in each subplot of the figure. Notably, all methods perform well in classifying normal samples. However, the distinguishing factor lies in the recall rates of defect labels. Our MPOFI framework exhibits higher recall rates for minority labels than other methods, emphasizing its superiority in handling imbalanced datasets and effectively identifying nonconforming threaded pipe connections in the manufacturing process.

V. CONCLUSION

This study introduces a novel deep metric learning framework tailored for the classification of imbalanced, multichannel, and partially observed functional data within the context of manufacturing processes. While prior research on classifying multichannel and partially observed functional data exists, addressing the challenge of imbalanced classification has not been adequately explored within the realm of functional data analysis. To facilitate an imbalanced classification, we propose a novel functional neural network that encodes multichannel and partially observed functional data, allowing it to be trained effectively on highly imbalanced datasets. Furthermore, the padding mechanism and contrastive loss associated with the functional neural network are specifically tailored to address the characteristics of functional data derived from manufacturing processes. We also provide comprehensive guidelines for tuning the hyperparameters of the framework to ensure optimal performance.

To validate the effectiveness of our MPOFI framework, we apply it to a real dataset derived from the manufacture of threaded pipe connections. The results demonstrate that MPOFI outperforms existing benchmark methods designed for partially observed functional data. This validation underscores the utility of our framework in achieving the accurate identification and classification of nonconforming threaded pipe connections in industrial manufacturing processes.

APPENDIX

A. Proofs for the Functional Neural Network $f(\cdot)$

In this section, we introduce the details and proofs for constructing the Toeplitz matrix form of $\boldsymbol{h}_{(c)}^{(l)}(t)$ and $\boldsymbol{H}_{(c)}(t)$ in the function neural network $f(\cdot)$. The Toeplitz matrix is a square matrix $\boldsymbol{P}^{N\times N}$ where the values along the negative sloping diagonals are equal. Given the first column $[p_0,\ldots,p_{N-1}]^T$ and first row $[p_0,\ldots,p_{N+1}]$, the matrix is in the following form:

$$\boldsymbol{P}^{N\times N} = \begin{bmatrix} p_0 & p_{-1} & p_{-2} & \cdots & p_{-N+2} & p_{-N+1} \\ p_1 & p_0 & p_{-1} & \cdots & p_{-N+3} & p_{-N+2} \\ p_2 & p_1 & p_0 & \cdots & p_{-N+4} & p_{-N+3} \\ \vdots & \vdots & \vdots & \ddots & \vdots & \vdots \\ p_{N-2} & p_{N-3} & p_{N-4} & \cdots & p_0 & p_{-1} \\ p_{N-1} & p_{N-2} & p_{N-3} & \cdots & p_1 & p_0 \end{bmatrix}.$$

For the functional data X(t), a Toeplitz matrix always exists for convolution weights $\boldsymbol{h}_{(c)}^{(l)}(t)$ given any length T of the functional input. Suppose the weights $\boldsymbol{h}_{(c)}^{(l)}(t)$ have a convolution kernel $\boldsymbol{w}_{(c)}^{(l)} = [w_1, ..., w_{k_w}]$ with kernel size k_w and dilation size d. The Toeplitz matrix is of size $T \times T$, and the matrix is derived by setting the value of p_n , n = 1, ..., T - 1 as the following:

$$p_n = 0, \forall n \neq r * 2^d, r = 0, ..., k_w - 1,$$

 $p_{r*2}^d = w_{k_w-r}, r = 0, ..., k_w - 1.$

For example, we set the kernel size $k_w = 3$ and the dilation size d = 1 for a functional input of length T = 6. The Toeplitz matrix is derived from the convolution kernel $[w_1, w_2, w_3]$ as:

$$\boldsymbol{h}_{(c)}^{(l)}(t) = \begin{bmatrix} w_3 & 0 & 0 & 0 & 0 & 0 \\ 0 & w_3 & 0 & 0 & 0 & 0 \\ w_2 & 0 & w_3 & 0 & 0 & 0 \\ 0 & w_2 & 0 & w_3 & 0 & 0 \\ w_1 & 0 & w_2 & 0 & w_3 & 0 \\ 0 & w_1 & 0 & w_2 & 0 & w_3 \end{bmatrix}.$$

It has to be noted that the formula for $h_{(c)}^{(l)}(t)$ does not consider the padded value of X(t). Therefore, the Toeplitz matrix of the convolution layer $h_{(c)}^{(l)}(t)$ is an approximation of the convolution operation. The approximation can be inaccurate when the padded length is considerable under a large dilation size d. Therefore, we apply the partial convolution [34] technique to deeper layers to alleviate the effect of padding. In each convolution operation, an element-wise multiplication is performed between the input $u_{(c)}^{(l-1)}(t)$ and a binary masking layer M, where the binary mask is zero if the corresponding region is a padded value.

$$\boldsymbol{u}_{(c)}^{(l)}(t) = \boldsymbol{b}_{(c)}^{(l)}(t) + \boldsymbol{h}_{(c)}^{(l)}(t) \left(\boldsymbol{M} \odot \boldsymbol{u}_{(c)}^{(l-1)}(t) \right) \frac{\|\mathbf{1}\|_{1}}{\|\boldsymbol{M}\|_{1}}$$

Moreover, we add a causal constraint to the convolution layers to accept only the padded value at the beginning of each input function. The padded values for X(t) when t > T are not involved because only the thread engagement phase at the beginning of each function is incomplete. Thus, each Toeplitz matrix is of the same size $T \times T$ and can be multiplied to obtain a matrix $H_{(c)}(t)$ representing all layers.

$$\mathbf{H}_{(c)}(t) = \mathbf{h}_{(c)}^{(D-1)}(t) \times \cdots \times \mathbf{h}_{(c)}^{(0)}(t),
\mathbf{u}_{(c)}^{(D-1)}(t) = \mathbf{b}_{(c)}(t) + \mathbf{H}_{(c)}(t)X(t).$$

The $H_{(c)}(t)$ is also a $T \times T$ matrix and can be adapted to functions X(t) of any lengths. We find that the input X(t), bias $b_{(c)}(t)$ and output $u_{(c)}^{(D-1)}(t)$ are all functional data. By transforming each column of the matrix $H_{(c)}(t)$ as a functional basis $\phi'_{(g)}(t)$ with its coefficient $a_g, g=1,...,T$, the result $H_{(c)}(t)X(t)$ can be interpreted as a linear combination of the product between basis functions $\left\{\phi'_{(g)}(t)\right\}$ and X(t).

$$\mathbf{H}_{(c)}(t) = [a_1 \phi'_{(1)}(t), a_2 \phi'_{(2)}(t), ..., a_T \phi'_{(T)}(t)],$$

$$\mathbf{H}_{(c)}(t) \mathbf{X}(t) = \sum_{g=1}^{T} a_g \phi'_{(g)}(t) \mathbf{X}(t).$$

Therefore, the Functional MLP structure $\boldsymbol{\beta}_{(c)}(t) = \{\boldsymbol{b}_{(c)}(t), \boldsymbol{H}_{(c)}(t)\}$ is a functional neural network that can accept and adapt to a functional input of any length without specifying the domain range.

REFERENCES

- [1] Vam Book, 2021. [Online]. Available: http://www.vamservices.com/Library/files/VAM%C2%AE%20Book.pdf.
- [2] Y. Guangjie, Y. Zhenqiang, W. Qinghua, and T. Zhentong, "Numerical and Experimental Distribution of Temperature and Stress Fields in Api Round Threaded Connection," *Engineering Failure Analysis*, vol. 13, no. 8, pp. 1275-1284, 2006.
- [3] X. Honglin, S. Taihe, and Z. Zhi, "Theoretical Analysis on Makeup Torque in Tubing and Casing Premium Threaded Connections," *Journal* of Southwest Petroleum University (Science & Technology Edition), vol. 36, no. 5, p. 160, 2014.
- [4] R. Mayne and S. Margolis, Introduction to Engineering. 1982.

> REPLACE THIS LINE WITH YOUR MANUSCRIPT ID NUMBER (DOUBLE-CLICK HERE TO EDIT) <

- [5] J. Du, X. Zhang, and J. Shi, "Pairwise Critical Point Detection Using Torque Signals in Threaded Pipe Connection Processes," *Journal of Manufacturing Science and Engineering*, vol. 139, no. 9, 2017.
- [6] J. Du, X. Zhang, and J. Shi, "A Physics-Specific Change Point Detection Method Using Torque Signals in Pipe Tightening Processes," *IEEE Transactions on Automation Science and Engineering*, vol. 16, no. 3, pp. 1289-1300, 2018.
- [7] J. Du, X. Zhang, X. Xu, and J. Shi, "A Novel Critical Point Detection Method for Mechanical Deformation in Tightening Processes," *Journal of Manufacturing Systems*, vol. 48, pp. 157-165, 2018.
- [8] J. Yao, J. Mueller, and J.-L. Wang, "Deep Learning for Functional Data Analysis with Adaptive Basis Layers," in *International Conference on Machine Learning*, 2021: PMLR, pp. 11898-11908.
- [9] G. M. James and T. J. Hastie, "Functional Linear Discriminant Analysis for Irregularly Sampled Curves," *Journal of the Royal Statistical Society: Series B (Statistical Methodology)*, vol. 63, no. 3, pp. 533-550, 2001.
- [10] A. Delaigle and P. Hall, "Classification Using Censored Functional Data," Journal of the American Statistical Association, vol. 108, no. 504, pp. 1269-1283, 2013.
- [11] D. Kraus, "Components and Completion of Partially Observed Functional Data," *Journal of the Royal Statistical Society: Series B: Statistical Methodology*, pp. 777-801, 2015.
- [12] A. Kneip and D. Liebl, "On the Optimal Reconstruction of Partially Observed Functional Data," *The Annals of Statistics*, vol. 48, pp. 1692-1717, 2020, Art no. 3.
- [13] C. Elkan, "The Foundations of Cost-Sensitive Learning," in *International Joint Conference on Artificial Intelligence*, 2001, vol. 17, no. 1: Lawrence Erlbaum Associates Ltd, pp. 973-978.
- [14] T.-Y. Lin, P. Goyal, R. Girshick, K. He, and P. Dollár, "Focal Loss for Dense Object Detection," in *Proceedings of the IEEE International Conference on Computer Vision*, 2017, pp. 2980-2988.
- [15] N. V. Chawla, K. W. Bowyer, L. O. Hall, and W. P. Kegelmeyer, "Smote: Synthetic Minority over-Sampling Technique," *Journal of Artificial Intelligence Research*, vol. 16, pp. 321-357, 2002.
- [16] G. E. Hinton and R. R. Salakhutdinov, "Reducing the Dimensionality of Data with Neural Networks," *Science*, vol. 313, no. 5786, pp. 504-507, 2006
- [17] A. Radford, L. Metz, and S. Chintala, "Unsupervised Representation Learning with Deep Convolutional Generative Adversarial Networks," arXiv preprint arXiv:1511.06434, 2015.
- [18] Y. Zhang, B. Kang, B. Hooi, S. Yan, and J. Feng, "Deep Long-Tailed Learning: A Survey," *IEEE Transactions on Pattern Analysis and Machine Intelligence*, 2023.
- [19] S. Mou, M. Cao, H. Bai, P. Huang, J. Shi, and J. Shan, "Paedid: Patch Autoencoder-Based Deep Image Decomposition for Pixel-Level Defective Region Segmentation," *IISE Transactions*, pp. 1-15, 2023.
- [20] P. Khosla et al., "Supervised Contrastive Learning," Advances in Neural Information Processing Systems, vol. 33, pp. 18661-18673, 2020.
- [21] P. Wang, K. Han, X.-S. Wei, L. Zhang, and L. Wang, "Contrastive Learning Based Hybrid Networks for Long-Tailed Image Classification," in *Proceedings of the IEEE/CVF Conference on Computer Vision and Pattern Recognition*, 2021, pp. 943-952.
- [22] J. Zhu, Z. Wang, J. Chen, Y.-P. P. Chen, and Y.-G. Jiang, "Balanced Contrastive Learning for Long-Tailed Visual Recognition," in Proceedings of the IEEE/CVF Conference on Computer Vision and Pattern Recognition, 2022, pp. 6908-6917.
- [23] K. Sohn, "Improved Deep Metric Learning with Multi-Class N-Pair Loss Objective," Advances in Neural Information Processing Systems, vol. 29, 2016.
- [24] A. Elías, R. Jiménez, A. M. Paganoni, and L. M. Sangalli, "Integrated Depths for Partially Observed Functional Data," *Journal of Computational and Graphical Statistics*, pp. 1-12, 2022.
- [25] J. Li, J. A. Cuesta-Albertos, and R. Y. Liu, "Dd-Classifier: Nonparametric Classification Procedure Based on Dd-Plot," *Journal of the American Statistical Association*, vol. 107, no. 498, pp. 737-753, 2012.
- [26] J. A. Cuesta-Albertos, M. Febrero-Bande, and M. Oviedo de la Fuente, "The Dd G-Classifier in the Functional Setting," *Test*, vol. 26, no. 1, pp. 119-142, 2017.
- [27] D. Kraus and M. Stefanucci, "Classification of Functional Fragments by Regularized Linear Classifiers with Domain Selection," *Biometrika*, vol. 106, no. 1, pp. 161-180, 2019.
- [28] J. Park, J. Ahn, and Y. Jeon, "Sparse Functional Linear Discriminant Analysis," *Biometrika*, vol. 109, no. 1, pp. 209-226, 2022.
- [29] Q. Wang, S. Zheng, A. Farahat, S. Serita, T. Saeki, and C. Gupta,

- "Multilayer Perceptron for Sparse Functional Data," in 2019 International Joint Conference on Neural Networks (IJCNN), 2019: IEEE, pp. 1-10.
- [30] A. v. d. Oord et al., "Wavenet: A Generative Model for Raw Audio," arXiv preprint arXiv:1609.03499, 2016.
- [31] J. Ramsay, J. Ramsay, and B. Silverman, Functional Data Analysis. Springer Science & Business Media, 2005.
- [32] J.-Y. Franceschi, A. Dieuleveut, and M. Jaggi, "Unsupervised Scalable Representation Learning for Multivariate Time Series," Advances in Neural Information Processing Systems, vol. 32, 2019.
- [33] L. Van der Maaten and G. Hinton, "Visualizing Data Using T-Sne," Journal of Machine Learning Research, vol. 9, no. 11, 2008.
- [34] G. Liu, F. A. Reda, K. J. Shih, T.-C. Wang, A. Tao, and B. Catanzaro, "Image Inpainting for Irregular Holes Using Partial Convolutions," in Proceedings of the European Conference on Computer Cision (ECCV), 2018, pp. 85-100.

> REPLACE THIS LINE WITH YOUR MANUSCRIPT ID NUMBER (DOUBLE-CLICK HERE TO EDIT) <

Yukun Xie received the B.S. degree in industrial engineering from the Shanghai Jiao Tong University, Shanghai, China, in 2021. He is currently pursuing the Ph.D. degree with the Smart Manufacturing Thrust, Systems Hub, The Hong Kong University of Science and Technology, Guangzhou, China.

His research interests include analysis, monitoring and diagnosis of industrial data, especially the profile data for quality inspection.

Juan Du (M'17) received the bachelor's degree in composite materials and engineering from the Harbin Institute of Technology, Harbin, China, in 2014, and the Ph.D. degree in management science and engineering from Peking University, Beijing, China, in 2019. From 2017 to 2019, she was a Visiting Scholar with the H. Milton Stewart School of Industrial and Systems Engineering, Georgia Institute of Technology, Atlanta, GA, USA.

She is currently an Assistant Professor with the Smart Manufacturing Thrust, Systems Hub, The Hong Kong University of Science and Technology (Guangzhou), China. She is also affiliated with the Department of Mechanical and Aerospace Engineering, The Hong Kong University of Science and Technology, Hong Kong SAR, China, and Guangzhou HKUST Fok Ying Tung Research Institute, Guangzhou, China. Her current research interests include data analytics and machine learning for modeling, monitoring, control, diagnosis and optimization in smart manufacturing systems. Dr. Du is a senior member of the Institute of Industrial and Systems Engineers (IISE).

Chen Zhang (Member, IEEE) is an Associate Professor in the Department of Industrial Engineering at Tsinghua University. She got her Ph.D. degree from National University of Singapore, and her B.E. degree from Tianjin University. Her primary research focus is on industrial data analysis based on statistics and artificial intelligence, includes modeling, causal inference, and online monitoring algorithms for complex systems.